Robust GNSS/INS Integrated Navigation Algorithm Based on Adaptive Factor Graph Optimization

Guoqiang Mao, ***Fellow, IEEE***
School of Transportation
Southeast University, Nanjing 210096, China
Email: g.mao@ieee.org

Keyin Wang, Corresponding Author
School of Telecommunications Engineering
Xidian University, Xi'an 710071, China
Email: keyinwang@stu.xidian.edu.cn

Tianxuan Fu
School of Telecommunications Engineering
Xidian University, Xi'an 710071, China
Email: futianxuan@stu.xidian.edu.cn

Word Count: 4955 words + 3 table(s) × 250 = 5705 words

Submission Date: December 2, 2025

ABSTRACT

The integration of the global navigation satellite system (GNSS) and inertial navigation system (INS) based on factor graph optimization (FGO) holds significant potential for achieving accurate and robust vehicle localization. However, in complex environments, the uncertainty of GNSS measurement noise severely affects the accuracy of state estimation in FGO. To address this problem, an adaptive FGO integrated navigation framework based on innovation-based adaptive estimation (IAE) is proposed. First, inertial measurement unit (IMU) preintegration factor, GNSS positioning factor, and prior factor are constructed for FGO. Then, an IAE-based approach, which estimates the GNSS measurement noise covariance matrix (MNCM) using innovations within a sliding time window, is introduced into the FGO framework to enable simultaneous estimation of vehicle states and measurement noise. To further enhance the accuracy of measurement noise estimation and the adaptability to varying conditions, a strategy based on innovation variance is adopted to dynamically adjust the size of the window for covariance estimation. The proposed method is evaluated through numerical simulations and real-world experiments. The experimental results demonstrate the effectiveness of the proposed approach in enhancing localization accuracy by accurately estimating time-varying GNSS measurement noise.

Keywords: Vehicle localization, global navigation satellite system (GNSS)/inertial navigation system (INS), factor graph optimization (FGO), innovation-based adaptive estimation (IAE)

INTRODUCTION

An accurate and reliable positioning system is critical for connected and autonomous vehicles (CAVs) (*1, 2*). On one hand, the positioning system provides the vehicle's location information, serving as the foundation for high-level decision-making and path planning tasks; on the other hand, by continuously updating the vehicle's position and perception data, the positioning system enables efficient interaction between the vehicle and its external environment (such as other vehicles, infrastructure, and cloud systems), ensuring the safety and stability of autonomous driving (*3–5*).

Due to the complementary advantages of the global navigation satellite system (GNSS) and the inertial navigation system (INS), the GNSS/INS integrated navigation system is widely used for positioning in CAVs (*6–8*). Traditional GNSS/INS integration is mostly based on the extended Kalman filter (EKF) (*9*), as well as more advanced filters that better handle nonlinearity, such as the unscented Kalman filter (UKF) (*10*), cubature Kalman filter (CKF) (*11*), and particle filter (PF) (*12*). In recent years, with the advancement of computing power, state estimation methods based on factor graph optimization (FGO) have become a research hotspot (*13*). FGO iteratively optimizes historical and current information in the form of factors to find the optimal state estimate, and when applied to integrated navigation, it often achieves higher positioning accuracy than traditional filtering methods (*14, 15*). In addition, the FGO framework offers high flexibility, enabling plug-and-play integration of sensor measurements, which makes it well-suited for multi-sensor fusion-based localization (*16*).

At its core, FGO estimates system states by minimizing a weighted error function, where the weights are determined by the covariance matrices of the observation noise. Therefore, the GNSS measurement error model directly affects the final integrated localization results of GNSS/INS (*17*). In most cases, the GNSS measurement error model is defined based on experiments or empirical knowledge (*18*). However, in real-world environments, GNSS measurements often exhibit time-varying characteristics, making it difficult to obtain an accurate error model (*19, 20*).

Currently, robust FGO methods for handling measurement noise uncertainty mainly include graph-based methods (*21, 22*) and M-estimators (*23, 24*). Graph-based methods enhance the robustness of the FGO by adding additional measurement constraints into the optimization process. Suenderhauf et al. (*25*) introduced Switch Constraints (SC) in FGO, which define an observation weighting function based on switch variables that dynamically adjust the weight of measurements according to the Mahalanobis distance between predicted and actual observations. This approach significantly improves localization accuracy in the presence of GNSS multipath measurements. Agarwal et al. (*22*) proposed an improved SC method called Dynamic Covariance Scaling (DCS), where the switch variables are removed from the optimization process and calculated separately using the residual, current measurement uncertainty, and prior switch uncertainty. After calculation, the information matrix associated with the GNSS observation factor is scaled accordingly. In addition to the aforementioned graph-based robust FGO methods, M-estimators-based methods are also widely used to handle measurement uncertainty in FGO. Unlike graph-based methods, M-estimators are based on the principle of maximum likelihood, where robust loss functions are introduced to reduce the weights of outlier measurements, thereby improving localization accuracy. Qin et al. (*26*) employed the Huber loss function to distinguish measurement outliers in a factor graph-based tightly coupled integrated navigation system, thereby enhancing the robustness of the system. Zhou et al. (*24*) combined M-estimator with chi-squared test to construct a scaling factor for adjusting GNSS measurement error covariance, thereby establishing a robust FGO framework that effectively handles outliers and time-varying measurement noise in complex environments. **Although existing robust FGO methods can partially address the measurement anomalies of GNSS signals, they lack the ability to estimate GNSS measurement noise and are ineffective in dealing with the time-varying characteristics of GNSS measurement noise.**

To address this limitation, we propose an adaptive FGO framework for GNSS/INS integration with time-varying measurement noise estimation. First, inertial measurement unit (IMU) preintegration factor, GNSS positioning factor, and prior factor are constructed for FGO. Then, we incorporate an innovation-based adaptive estimation (IAE) method into the FGO framework, where the GNSS measurement noise covariance matrix (MNCM) is estimated from innovations within a sliding time window, to jointly estimate the system states and measurement noise. Furthermore, to improve the robustness and accuracy of noise estimation under varying conditions, the window size for covariance estimation is dynamically adjusted according to the innovation variance. In this way, the proposed method enables joint estimation of navigation states and GNSS measurement noise, thereby improving the accuracy of GNSS/INS integrated localization. The main contributions of this paper can be summarized as follows:

1. A measurement noise estimation method based on IAE is introduced into the FGO framework to jointly estimate the system states and the GNSS MNCM, thereby improving the localization accuracy of FGO-based GNSS/INS integrated navigation system.
2. A strategy based on innovation variance is proposed to dynamically adjust the window size for covariance estimation, enhancing both the robustness and accuracy of GNSS measurement noise estimation.
3. Extensive experiments in the form of both numerical simulations and real-world tests are conducted. Experimental results demonstrate that the proposed adaptive FGO algorithm with measurement noise estimation significantly enhances the positioning accuracy of GNSS/INS integrated navigation.

The remainder of this paper is organized as follows. First, an FGO-based GNSS/INS integrated navigation system is given. Next, details on the IAE-based adaptive FGO method are provided. Then, the experimental results are presented. Finally, the conclusion and future work are discussed.

FGO-BASED GNSS/INS INTEGRATED NAVIGATION SYSTEM

The objective of multi-sensor information fusion is to compute the maximum a posteriori (MAP) probability of the system state given all available sensor measurements. In this study, the measurement information includes GNSS measurements and IMU measurements. The GNSS/INS integrated navigation problem can be represented as follows:

$$x^* = \arg\max_x \prod_k P(z_k^{\text{sensor}}|x_k) \prod_k P(x_k|x_{k-1}) \tag{1}$$

where x^* denotes the optimal state estimation, z_k^{sensor} is the measurement value from sensors at time k, and x_k and x_{k-1} denote the system state at times k and $k-1$, respectively.

To obtain the solution to (1), Bayesian filtering adopts a first-order Markov model, estimating the current state based on the previous state and the current observations. In contrast, FGO transforms this problem into a nonlinear optimization problem through the structure of the factor graph. In FGO, all sensor measurements are treated as constraints associated with specific states (*27*). In this context, the MAP problem can be expressed as follows:

$$x^* = \arg\max_x \prod_i f_i(x_i) \tag{2}$$

where f_i denotes the factor associated with the measurement information. Assuming that the noise from all sensors follows Gaussian distributions, f_i can be expressed as follows:

$$f_i(x_i) \propto \exp\left(-\|h_i(x_i) - z_i^{\text{sensor}}\|^2_{\Sigma_i}\right) \tag{3}$$

where $h_i(\cdot)$ denotes the observation equation, whose specific form depends on the particular model, and Σ_i is the noise covariance matrix of the corresponding sensor. The MAP problem in (1) can be further transformed as follows:

$$x^* = \arg\max_x \left(\sum_i \|h_i(x_i) - z_i^{\text{sensor}}\|^2_{\Sigma_i}\right). \tag{4}$$

The state x_k in this study is defined as follows:

$$x_k = \left[p^w_{wb_k}, v^w_{wb_k}, q^w_{wb_k}, b_{g_k}, b_{a_k}\right]^T \tag{5}$$

where the superscript w denotes the world frame (w-frame), which is defined at the initial position of the navigation system in the north-east-down (NED) coordinate system, the subscript b denotes the body frame (b-frame), $p^w_{wb_k}$, $v^w_{wb_k}$, and $q^w_{wb_k}$ represent the position, velocity, and rotation of the b-frame with respect to the w-frame expressed in the w-frame, respectively, and b_{g_k} and b_{a_k} represent the gyroscope and accelerometer biases, respectively.

In the factor graph, adjacent states are connected by IMU preintegration factors, which model the evolution of the system state over time. GNSS positioning factors are linked to each state node to provide absolute position constraints, effectively correcting the drift inherent in INS. To limit the size of the optimization problem, marginalization is applied, which introduces prior factors that transfer historical information constraints into the current optimization window. In the following sections, we will detail the specific form of each factor.

IMU Preintegration Factor

In general, the sampling frequency of the IMU is much higher than that of the GNSS. To avoid repeatedly integrating the high-frequency IMU data during optimization, the IMU measurements within each GNSS sampling interval are typically preintegrated. This approach effectively improves the optimization efficiency of the integrated navigation.

The IMU measurement model can be expressed as follows:

$$\begin{cases} \tilde{\omega}_{ib}^{b} = \omega_{ib}^{b} + b_g + n_g \\ \tilde{f}^{b} = f^{b} + b_a + n_a \end{cases} \tag{6}$$

where the subscript i denotes the inertial frame (i-frame), $\tilde{\omega}_{ib}^{b}$ and $\tilde{f}^{b}$ are the measured angular rate of the b-frame relative to the i-frame expressed in the b-frame and the measured specific force, respectively, ω_{ib}^{b} and f^{b} are the true angular rate of the b-frame relative to the i-frame expressed in the b-frame and the true specific force, respectively, b_g and b_a represent the gyroscope and accelerometer biases, respectively, and n_g and n_a represent the gyroscope and accelerometer white noise, respectively.

Based on the IMU measurements, the angular and velocity increments between consecutive IMU samples can be expressed as follows:

$$\begin{cases} \Delta\theta_m = \int_{t_{m-1}}^{t_m} \hat{\omega}_{ib}^{b}\, dt \\ \Delta v_{f,m}^{b} = \int_{t_{m-1}}^{t_m} \hat{f}^{b}\, dt \end{cases} \tag{7}$$

where $\hat{\omega}_{ib}^{b}$ and $\hat{f}^{b}$ represent the angular rate and specific force after compensating for the estimated gyroscope bias $\hat{b}_g$ and accelerometer bias $\hat{b}_a$, respectively, $\hat{\omega}_{ib}^{b} = \tilde{\omega}_{ib}^{b} - \hat{b}_g$, and $\hat{f}^{b} = \tilde{f}^{b} - \hat{b}_a$.

The motion integration equations can be expressed as follows:

$$\begin{cases} q_{wb(t_m)}^{w} = q_{wb(t_{m-1})}^{w} \otimes q_{\Delta\theta_m} \\ v_{wb(t_m)}^{w} = v_{wb(t_{m-1})}^{w} + R_{wb(t_{m-1})}^{w} \Delta v_{f,m}^{b} + g^{w} \Delta t_{m-1,m} \\ p_{wb(t_m)}^{w} = p_{wb(t_{m-1})}^{w} + v_{wb(t_{m-1})}^{w} \Delta t_{m-1,m} + \frac{1}{2}\left(R_{wb(t_{m-1})}^{w} \Delta v_{f,m}^{b} + g^{w}\right) \Delta t_{m-1,m} \end{cases} \tag{8}$$

where the subscripts t_m and t_{m-1} represent the IMU sampling times, $\Delta t_{m-1,m} = t_m - t_{m-1}$, $q_{\Delta\theta_m}$ is the quaternion for the incremental angle $\Delta\theta_m$, p_{wb}^{w}, v_{wb}^{w}, and q_{wb}^{w} represent the position, velocity, and rotation of the b-frame with respect to the w-frame expressed in the w-frame, respectively, R_{wb}^{w} is the rotation matrix from b-frame to w-frame expressed in the w-frame, g^{w} is the gravitational acceleration, and $\otimes$ denotes quaternion multiplication.

By integrating the IMU measurements over the GNSS sampling interval using (8), the IMU preintegration measurements can be obtained as follows:

$$\begin{cases} q_{k-1,k}^{\text{Pre}} = \prod_{m\in[k-1,k]} q_{\Delta\theta_m} \\ v_{k-1,k}^{\text{Pre}} = \sum_{m\in[k-1,k]} \left(R_{wb(t_{m-1})}^{w} \Delta v_{f,m}^{b} + g^{w} \Delta t_{m-1,m}\right) \\ p_{k-1,k}^{\text{Pre}} = \sum_{m\in[k-1,k]} \left(v_{wb(t_{m-1})}^{w} \Delta t_{m-1,m} + \frac{1}{2} R_{wb(t_{m-1})}^{w} \Delta v_{f,m}^{b} \Delta t_{m-1,m} + \frac{1}{2} g^{w} \Delta t_{m-1,m}\right) \end{cases} \tag{9}$$

where $q_{k-1,k}^{\text{Pre}}$, $v_{k-1,k}^{\text{Pre}}$, and $p_{k-1,k}^{\text{Pre}}$ denote the attitude preintegration, velocity preintegration, and position preintegration from time $k-1$ to time k, respectively.

Based on the above derivation, the IMU preintegration residual, i.e., the IMU preintegration factor, can be computed as follows:

$$\mathbf{r}_{\text{Pre}}(\hat{z}_{k-1,k}^{\text{Pre}}, X) = \begin{bmatrix} p_{wb_k}^w - p_{wb_{k-1}}^w - v_{wb_{k-1}}^w \Delta t_{k-1,k} - \frac{1}{2} g^w \Delta t_{k-1,k}^2 - \mathbf{R}_{b_{k-1}}^w p_{k-1,k}^{\text{Pre}} \\ v_{wb_k}^w - v_{wb_{k-1}}^w - g^w \Delta t_{k-1,k} - \mathbf{R}_{b_{k-1}}^w v_{k-1,k}^{\text{Pre}} \\ 2\left[\left(\mathbf{q}_{b_{k-1}}^w \right)^{-1} \otimes \mathbf{q}_{b_k}^w \otimes \left(\mathbf{q}_{k-1,k}^{\text{Pre}} \right)^{-1} \right]_v \\ b_{g_k} - b_{g_{k-1}} \\ b_{a_k} - b_{a_{k-1}} \end{bmatrix} \tag{10}$$

where $2\left[\bullet\right]_v$ is the algorithm to extract the rotation vector from a quaternion.

The covariance matrix $\Sigma_{k-1,m}^{\text{Pre}}$ of the IMU preintegration factor can be propagated from the initial covariance $\Sigma_{k-1,k-1}^{\text{Pre}} = 0$ as follows:

$$\Sigma_{k-1,m}^{\text{Pre}} = \Phi_m \Sigma_{k-1,m-1}^{\text{Pre}} \Phi_m^T + Q_m \tag{11}$$

where $\Phi_m \approx \mathbf{I} + F_{t_{m-1}} \Delta t_{m-1,m}$, $F_{t_{m-1}}$ is the dynamics matrix, $Q_m \approx G_{t_{m-1}} Q_{t_{m-1}} G_{t_{m-1}}^T \Delta t_{m-1,m}$, $G_{t_{m-1}}$ is the noise-input mapping matrix, and $Q_{t_{m-1}}$ is the noise covariance matrix.

GNSS Positioning Factor

The position output from the GNSS receiver in the geographic frame $\hat{z}_k^{\text{GNSS}}$ can be transformed into the w-frame. Considering the lever-arm effect, the GNSS positioning factor can be formulated as follows:

$$r_{\text{GNSS}}\left(\hat{z}_k^{\text{GNSS}}, X\right) = p_{wb_k}^w + R_{wb_k}^w l_{\text{GNSS}}^b - \hat{p}_k^w \tag{12}$$

where l_{GNSS}^b is the GNSS antenna lever-arm expressed in the b-frame, $\hat{p}_k^w$ is the position of $\hat{z}_k^{\text{GNSS}}$ transformed from the geographic frame to the w-frame.

Prior Factor and Sliding Window Optimization

Given the IMU preintegration factor and GNSS positioning factor, the GNSS/INS integrated localization problem can be formulated as a MAP problem as shown in (4). As time progresses, the size of the factor graph increases, which leads to a slower optimization process. To limit the size of the factor graph, a sliding window approach is employed to constrain the number of epochs involved in the optimization. When the number of epochs exceeds the window size, the factors from the earliest epoch are marginalized, and the historical information is incorporated into the current optimization window in the form of prior factors. More details on the marginalization can be found in (*28*). By combining the IMU preintegration factor, GNSS positioning factor, and prior factor, the objective function to be optimized is constructed as follows:

$$\min_{X}\left\{\left\|r_p - H_pX\right\|^2 + \sum_{k\in[1,j]}\left\|r_{\mathrm{Pre}}\left(\hat{z}^{\mathrm{Pre}}_{k-1,k}, X\right)\right\|^2_{\Sigma^{\mathrm{Pre}}_{k-1,k}} + \sum_{i\in[0,g]}\left\|r_{\mathrm{GNSS}}\left(\hat{z}^{\mathrm{GNSS}}_{i}, X\right)\right\|^2_{\Sigma^{\mathrm{GNSS}}_{i}}\right\} \tag{13}$$

where $\{r_p, H_pX\}$ represents the prior information from the marginalization, $\left\|r_p - H_pX\right\|^2$ is the prior factor, j is the number of IMU preintegration factors, and $g+1$ ($g \leq j$) is the number of GNSS positioning factors. Σ_k^{GNSS} is the covariance matrix of GNSS position measurements. Its estimation process will be detailed in the next section.

IAE-BASED ADAPTIVE FGO

To enable simultaneous estimation of system states and GNSS measurement noise, we propose an adaptive FGO framework based on IAE. This method leverages the statistical characteristics of the innovation sequence within a sliding time window to estimate the GNSS MNCM, which is then integrated into the FGO framework to enhance pose estimation accuracy. To further enhance the accuracy and robustness of measurement noise estimation, we dynamically adjust the size of the sliding window used for covariance estimation based on the innovation variance.

IAE-Based Noise Covariance Estimation

The GNSS MNCM $\mathbf{R}_k$ is estimated using an innovation-based approach, which leverages the innovation sequence to capture time-varying noise characteristics. The innovation at time step k is defined as follows:

$$v_k = \mathbf{z}_k - H_k\hat{\mathbf{x}}_{k|k-1} \tag{14}$$

where z_k refers to the GNSS measurement at time step k, H_k is the Jacobian matrix of the GNSS measurement function, and $\hat{\mathbf{x}}_{k|k-1}$ is the predicted state vector, obtained from the previous state and the IMU preintegration. The innovation covariance S_k is theoretically given by

$$S_k = H_kP_{k|k-1}H_k^T + R_k \tag{15}$$

where $P_{k|k-1}$ is the prior state covariance, which comes from the inverse of the information matrix H_p in the marginalization operation. An empirical estimate of S_k can also be obtained over a window of M_k innovations as follows:

$$\hat{S}_k = \frac{1}{M_k}\sum_{i=k-M_k+1}^{k} v_i v_i^{\top}. \tag{16}$$

The measurement noise covariance is then estimated as follows:

$$\hat{R}_k = \hat{S}_k - H_k P_{k|k-1} H_k^T. \tag{17}$$

In practical scenarios, GNSS noise typically changes slowly. Considering this characteristic of GNSS noise, a forgetting factor α is used to assign certain weight to historical data, i.e.:

$$\hat{R}_k \leftarrow (1-\alpha)\hat{R}_{k-1} + \alpha \hat{R}_k \tag{18}$$

where α can be set empirically. In this study, α is set to 0.9.

Adaptive Window Size Adjustment

Unlike traditional methods with fixed window size for covariance estimation in IAE, we propose a strategy that adjusts M_k online based on the innovation variance. The innovation variance is computed as follows:

$$\mathrm{var}(\nu) = \frac{1}{n}\sum_{i=1}^{n} \|\nu_i - \bar{\nu}\|_2^2 \tag{19}$$

where n is the number of innovations in the window for covariance estimation, and $\bar{\nu}$ is the mean innovation.

Based on (19), it is evident that the larger the variance of ν, the greater the fluctuation in GNSS data quality within the window. To more accurately reflect the noise characteristics of the data, a larger window is required to compute its statistical features. Conversely, when the ν is smaller, it indicates that the GNSS data quality fluctuates less within the window. In this case, considering computational efficiency, a smaller window can be used to compute the statistical features. The window size M_k is adjusted according to the following rule:

$$M_k = \begin{cases} M_{\max} & \text{if } \mathrm{var}(\nu) > \nu_{\max} \\ \frac{1}{2}(M_{\max} + M_{\min}) & \text{if } \nu_{\min} < \mathrm{var}(\nu) \leq \nu_{\max} \\ M_{\min} & \text{if } \mathrm{var}(\nu) \leq \nu_{\min} \end{cases} \tag{20}$$

where $M_{\max}$, $M_{\min}$, $\nu_{\max}$, and $\nu_{\min}$ are the predefined maximum and minimum values of the window size and the variance, respectively. The settings of $\nu_{\max}$ and $\nu_{\min}$ should take into account the quality of the GNSS receiver and external environmental factors that may affect GNSS measurement quality. $M_{\min}$ should be sufficient to capture the statistical characteristics of the measurement data, while $M_{\max}$ should be set with consideration for computational resource limitations.

Compared to standard IAE method, where the window size remains constant throughout the estimation process, the proposed approach requires additional calculations for adjusting the window size based on the variance of the innovation sequence. However, the computa-

tional overhead introduced by this adaptive strategy is relatively moderate. The calculation of the innovation variance and the adjustment of the window size primarily involve simple arithmetic operations and are performed at each step in the process. These operations can be computed efficiently, especially when the window size adjustment is not highly dynamic. The key benefit is that the adaptive window allows for a more accurate reflection of GNSS noise characteristics, leading to improved pose estimation accuracy, which can justify the additional computational cost. Moreover, the adaptive strategy ensures that the size of the window is tailored to the quality of the GNSS measurements, which can also enhance computational efficiency by reducing the window size when the GNSS data quality is consistent. This results in fewer data points being processed for covariance estimation in high-quality data scenarios, thereby reducing the overall computational load.

EXPERIMENTAL RESULTS

To sufficiently validate the effectiveness of the proposed method, numerical simulations and real-world tests are conducted. In this section, we provide a detailed description of the experimental setups and corresponding results.

Numerical Simulations

To evaluate the proposed adaptive FGO method for estimating time-varying GNSS measurement noise, a vehicle simulation trajectory is designed. The simulation lasts for 320 seconds, during which the GNSS measurement noise covariance is set to $diag(100\,\mathrm{m}^2, 100\,\mathrm{m}^2)$ between 160 and 240 seconds, and $diag(1\,\mathrm{m}^2, 1\,\mathrm{m}^2)$ for the remaining periods. The GNSS sampling rate is 1 Hz, and the IMU parameters are listed in Table 1. **The maximum window size $M_{\mathbf{max}}$ is set to 20, and the minimum window size $M_{\mathbf{min}}$ is set to 10.**

To demonstrate the superiority of the proposed adaptive FGO based on IAE (IAE-FGO) in estimating GNSS measurement noise, we compare it with the estimation results obtained from adaptive filtering methods based on Sage-Husa (*29*) (Sage-Husa-Filter) and IAE (*30*) (IAE-Filter). In addition, to validate the effectiveness of the adaptive window size adjustment strategy proposed in this paper, we also provide the results of the FGO based on the IAE method with a fixed window size (IAE-FGO-Fix). The GNSS noise standard deviation estimates from different algorithms are shown in Figure 1. The root mean square error (RMSE) is used to measure the difference between estimated results and the ground truth, which is defined as follows:

$$\mathrm{RMSE} = \sqrt{\frac{1}{n}\sum_{i=1}^{n}(\hat{y}_i - y_i)^2} \tag{21}$$

where $\hat{y}_i$ is the output of the localization algorithm, y_i is the ground truth, and n is the total number of data. The RMSE of GNSS measurement noise standard deviation for different algorithms are summarized in Table 2.

It is evident that when the GNSS measurement noise remains constant, the Sage-Husa-based method can reliably estimate the measurement noise covariance. However, when the GNSS measurement noise varies, the Sage-Husa method struggles to track these changes. The methods based on IAE are capable of estimating time-varying GNSS measurement noise. The GNSS measurement noise estimation based on FGO achieves higher accuracy than that based on filtering.

This is because FGO jointly optimizes a larger amount of historical information, leading to more accurate state estimation. As a result, the innovations are more precise, which in turn improves the estimation accuracy of the GNSS MNCM. By adaptively adjusting the window size for covariance estimation, the estimation accuracy of the GNSS MNCM can be further improved. According to Table 2, compared to IAE-FGO-Fix, the IAE-FGO method reduces the RMSE of the GNSS measurement noise standard deviation by 6.25% in the east direction and 21.90% in the north direction, respectively.

TABLE 1 Specifications of IMU

Parameters	Unit	Value
Sample Rate	Hz	100
Gyro Bias Stability	°/h	8
Gyro Random Walk	$°/\sqrt{\mathrm{h}}$	0.4
Accelerometer Bias Stability	μg	30
Velocity Random Walk	$\mathrm{m/s}/\sqrt{\mathrm{h}}$	0.02

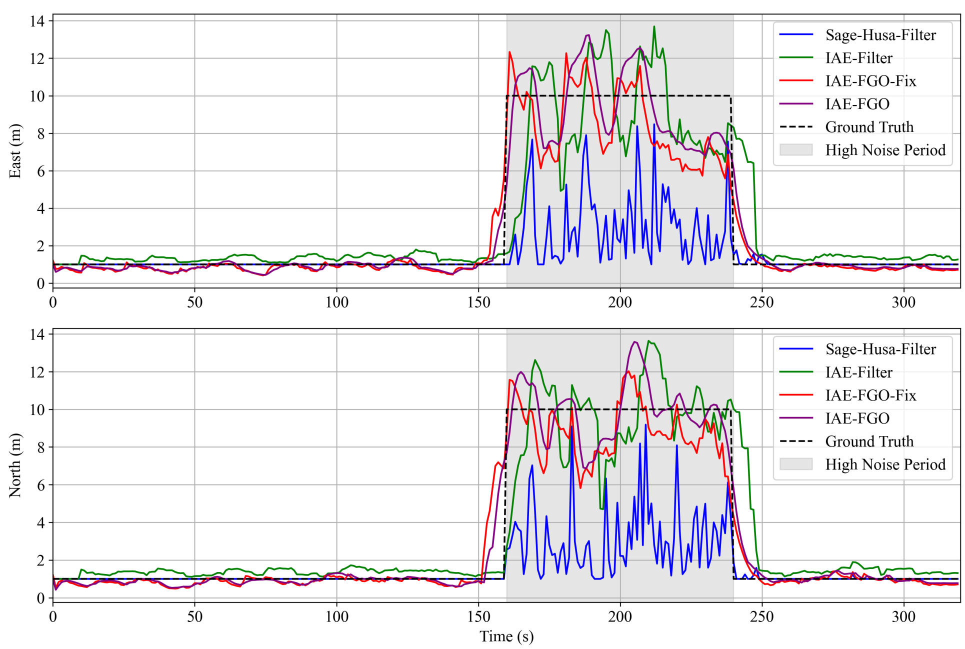

Figure 1 GNSS measurement noise standard deviation estimated by different algorithms.

Real-World Tests

To validate the effectiveness of the proposed positioning method in real-world scenarios, we set up a data acquisition experimental platform as shown in Figure 2. The platform includes a GNSS receiver (Topgnss, GNSS 100G) and an integrated navigation system (Xsens, MTi-680G). The integrated navigation system is mounted on the internal platform in the trunk of the vehicle,

TABLE 2 RMSE (m) of GNSS Measurement Noise Standard Deviation for Different Algorithms

Orientation	Sage-Husa-Filter	IAE-Filter	IAE-FGO-Fix	IAE-FGO
East	3.65	1.86	1.28	1.20
North	3.55	1.65	1.37	1.07

while the GNSS receiver is mounted on the roof of the vehicle. The system combines IMU and real-time kinematic (RTK) to provide reference data. The GNSS sampling frequency is 1 Hz, while the IMU operates at a frequency of 100 Hz. The bias stability of the gyroscopes and the accelerometers are $8\,^\circ/\mathrm{h}$ and $15\,\mu\mathrm{g}$, respectively, and the random walk of the gyroscopes and the velocity are $0.17\,^\circ/\sqrt{\mathrm{h}}$ and $0.02\,\mathrm{m/s}/\sqrt{\mathrm{h}}$, respectively. Screenshots of the real-world experimental environment are shown in Figure 3.

To illustrate the superiority of the proposed method (IAE-FGO) in state estimation accuracy, the robust FGO algorithm based on the Huber function (Huber-FGO) (*31*), the traditional FGO algorithm (*32*) and EKF (*14*) are used for comparison. Figure 4 shows the trajectory comparison of different algorithms. Figure 5 displays the positioning errors in the north, east, and down directions for different algorithms. The mean absolute positioning error (Mean Abs. Pos. Error), the maximum absolute positioning error (Max. Abs. Pos. Error), and the RMSE of the positioning results along different coordinate directions for different algorithms are reported in Table 3.

It is clearly evident that among the three positioning algorithms, FGO outperforms EKF in terms of positioning accuracy. This is because EKF only considers the state at the previous time step and the current measurements when performing state estimation, whereas FGO optimizes all states within the sliding optimization window to obtain the optimal value for the current state. **By introducing the Huber function, Huber-FGO improves the robustness of the traditional FGO in handling outliers or noisy data, thereby enhancing the accuracy of state estimation. The positioning accuracy achieved by the proposed IAE-FGO is the highest. This is because IAE-FGO can simultaneously estimate both the state and GNSS measurement noise, thereby achieving better state estimation results. According to Table 3, the RMSE of IAE-FGO's positioning results in the north, east, and down directions has improved by** 17.64 %**,** 12.73 %**, and** 5.71 %**, compared to Huber-FGO, respectively.**

CONCLUSION AND FUTURE WORK

This paper proposed an adaptive FGO framework based on IAE to address the challenge of GNSS measurement noise uncertainty in GNSS/INS integrated navigation system. First, the IMU preintegration factor, GNSS positioning factor, and prior factor were constructed for FGO. Then, the IAE method was incorporated into the FGO framework to allow for the simultaneous estimation of both states and the GNSS MNCM. To further improve the accuracy of measurement noise estimation and enhance adaptability to varying conditions, this work introduced a dynamic window adjustment strategy, which leveraged the variance of the innovation to dynamically adjust the window size for covariance estimation. Numerical simulations and real-world experiments validated the superiority of the proposed method. Specifically, in real-world experimental scenarios, the proposed method outperformed existing robust FGO, with positioning RMSE improvements in

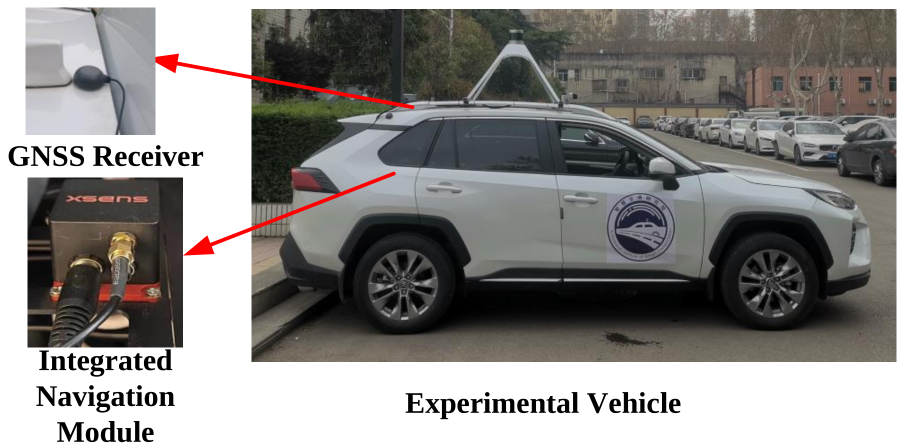

Figure 2 Experimental platform.

Figure 3 Screenshots of the real-world experimental environment.

the north, east, and down directions by 17.64%, 12.73%, and 5.71%, respectively.

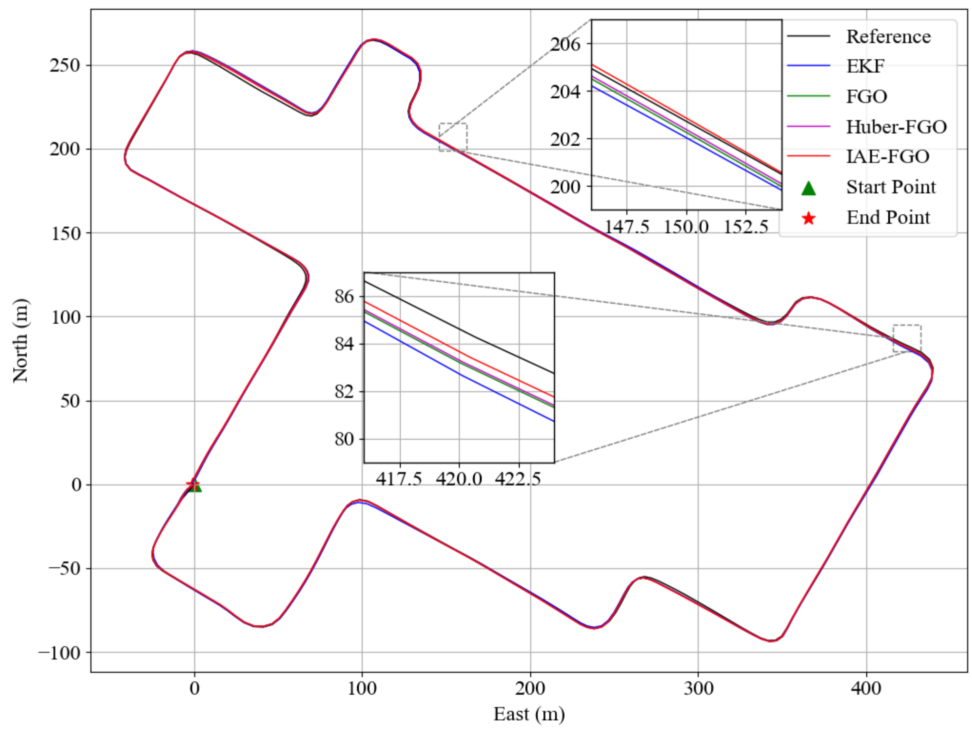

Figure 4 Trajectory comparison of different algorithms.

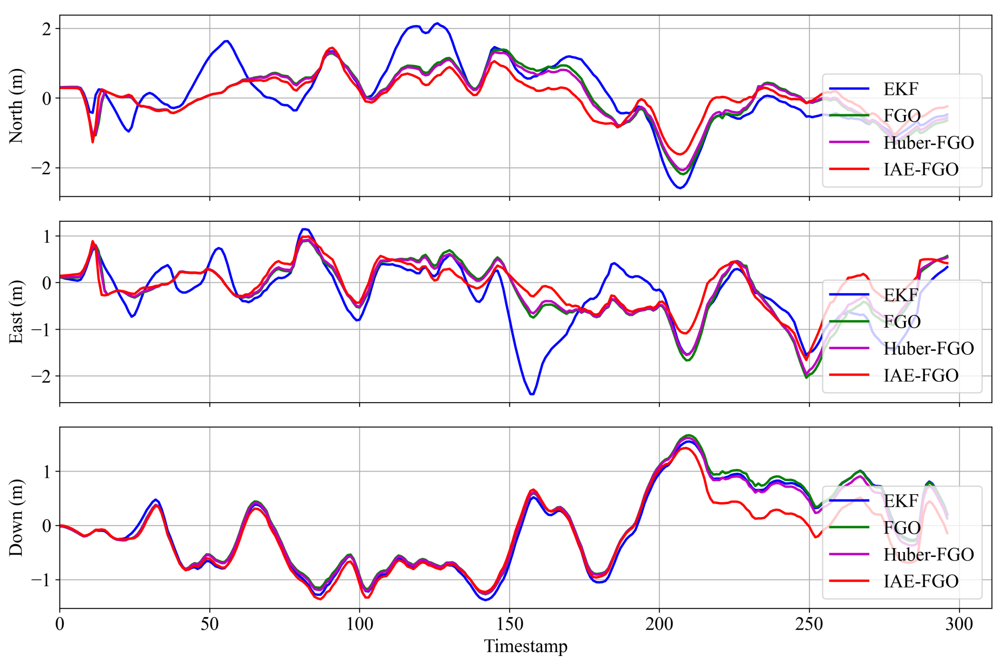

Figure 5 Positioning errors in the north, east, and down directions for different algorithms.

However, the method proposed in this paper also has its limitations. The IAE method estimates GNSS measurement noise based on data within a historical time window. In scenarios

TABLE 3 Performance of Different Algorithms

Method	Orientation	Mean Abs. Pos. Error (m)	Max. Abs. Pos. Error (m)	RMSE (m)
	North	0.75	2.59	0.96
EKF	East	0.55	2.39	0.74
	Down	0.75	1.55	0.75
	North	0.62	2.19	0.77
FGO	East	0.51	2.04	0.65
	Down	0.63	1.66	0.73
	North	0.56	2.06	0.68
Huber-FGO	East	0.46	1.96	0.55
	Down	0.60	1.58	0.70
	North	0.43	1.62	0.56
IAE-FGO	East	0.38	1.66	0.48
	Down	0.54	1.43	0.66

where GNSS measurement quality changes rapidly, this may lead to tracking delays. Enhancing the algorithm's ability to track noise variations more promptly will be a key focus of our future research.

AUTHOR CONTRIBUTIONS

The authors confirm contribution to the paper as follows: study conception and design: G. Mao; data collection: K. Wang, T. Fu; analysis and interpretation of results: G. Mao, K. Wang; draft manuscript preparation: G. Mao. K. Wang. All authors reviewed the results and approved the final version of the manuscript.

DECLARATION OF CONFLICTING INTERESTS

The authors declared no potential conflicts of interest with respect to the research, authorship, and/or publication of this article.

FUNDING

This research was supported by NSFC grant (Grant no. U21A20446).

REFERENCES

1. Tao, X., B. Zhu, S. Xuan, J. Zhao, H. Jiang, J. Du, and W. Deng, A Multi-Sensor Fusion Positioning Strategy for Intelligent Vehicles Using Global Pose Graph Optimization. *IEEE Transactions on Vehicular Technology*, Vol. 71, No. 3, 2022, pp. 2614–2627.
2. Li, Y., X. Zhang, X. Li, Z. Chen, Y. Hu, J. Yang, and A. Schmeink, Cooperative Elliptic Positioning Through Single UAV During GNSS Outages. *IEEE Transactions on Wireless Communications*, Vol. 23, No. 10, 2024, pp. 12749–12764.
3. Mahmoud, A., A. Noureldin, and H. S. Hassanein, Integrated Positioning for Connected Vehicles. *IEEE Transactions on Intelligent Transportation Systems*, Vol. 21, No. 1, 2020, pp. 397–409.
4. Ansari, K., Cooperative Position Prediction: Beyond Vehicle-to-Vehicle Relative Positioning. *IEEE Transactions on Intelligent Transportation Systems*, Vol. 21, No. 3, 2020, pp. 1121–1130.
5. Li, X., Z. Qin, Z. Shen, X. Li, Y. Zhou, and B. Song, A High-Precision Vehicle Navigation System Based on Tightly Coupled PPP-RTK/INS/Odometer Integration. *IEEE Transactions on Intelligent Transportation Systems*, Vol. 24, No. 2, 2023, pp. 1855–1866.
6. Tao, Z., Z. Li, Z. Chen, C. Pan, and W. Li, A Lightweight Motion Constraint Regulator for Enhanced GNSS/INS Tightly Coupled Integration in Urban Environments. *IEEE Transactions on Instrumentation and Measurement*, Vol. 74, 2025, pp. 1–15.
7. Meng, X., H. Tan, P. Yan, Q. Zheng, G. Chen, and J. Jiang, A GNSS/INS integrated navigation compensation method based on CNN GRU IRAKF hybrid model during GNSS outages. *IEEE Trans. Instrum. Meas.*, Vol. 73, 2024, pp. 1–15.
8. Xu, Y., K. Wang, C. Yang, Z. Li, F. Zhou, and D. Liu, GNSS/INS/OD/NHC adaptive integrated navigation method considering the vehicle motion state. *IEEE Sensors Journal*, Vol. 23, No. 12, 2023, pp. 13511–13523.
9. Chen, Q., Q. Zhang, and X. Niu, Estimate the pitch and heading mounting angles of the IMU for land vehicular GNSS/INS integrated system. *IEEE Transactions on Intelligent Transportation Systems*, Vol. 22, No. 10, 2021, pp. 6503–6515.
10. Julier, S. and J. Uhlmann, Unscented filtering and nonlinear estimation. *Proceedings of the IEEE*, Vol. 92, No. 3, 2004, pp. 401–422.
11. Arasaratnam, I. and S. Haykin, Cubature Kalman Filters. *IEEE Transactions on Automatic Control*, Vol. 54, No. 6, 2009, pp. 1254–1269.
12. Zhong, Y., X. Chen, Y. Zhou, and J. Wang, Adaptive Particle Filtering With Variational Bayesian and Its Application for INS/GPS Integrated Navigation. *IEEE Sensors Journal*, Vol. 23, No. 17, 2023, pp. 19757–19770.
13. Ben, Y., K. Wang, and Q. Li, A Robust Factor Graph Optimization Method for Navigation in Land Vehicles Based on Dynamic Kernel Principal Component Analysis. *IEEE Transactions on Instrumentation and Measurement*, Vol. 73, 2024, pp. 1–16.
14. Wen, W., Y. C. Kan, and L.-T. Hsu, Performance Comparison of GNSS/INS Integrations Based on EKF and Factor Graph Optimization. In *Proc. 32nd Int. Tech. Meeting Sat. Div. Inst. Navigation (ION GNSS+)*, Inst Navigat, Satellite Div, 2019, pp. 3019–3032.
15. Li, Z., J. Tao, Z. Lei, J. Guo, Q. Zhao, and X. Guo, Factor Graph Optimization-Based RTK/INS Integration With Raw Observations for Robust Positioning in Urban Canyons. *IEEE Transactions on Instrumentation and Measurement*, Vol. 74, 2025, pp. 1–11.

16. Bai, S., J. Lai, P. Lyu, B. Ji, B. Wang, and X. Sun, A Novel Plug-and-Play Factor Graph Method for Asynchronous Absolute/Relative Measurements Fusion in Multisensor Positioning. *IEEE Transactions on Industrial Electronics*, Vol. 70, No. 1, 2023, pp. 940–950.
17. Qiu, Z., S. Wang, P. Hu, and L. Guo, Outlier-Robust Extended Kalman Filtering for Bioinspired Integrated Navigation System. *IEEE TRANSACTIONS ON AUTOMATION SCIENCE AND ENGINEERING*, Vol. 21, No. 4, 2024, pp. 5881–5894.
18. Fan, G., Q. Wang, G. Yang, and P. Liu, RFG-TVIU: robust factor graph for tightly coupled vision/IMU/UWB integration. *FRONTIERS IN NEUROROBOTICS*, Vol. 18, 2024.
19. Li, X., Z. Qin, Z. Shen, X. Li, Y. Zhou, and B. Song, A high-precision vehicle navigation system based on tightly coupled PPP-RTK/INS/odometer Integration. *IEEE Trans. Intell. Transp. Syst.*, Vol. 24, No. 2, 2023, pp. 1855–1866.
20. Du, S., Y. Huang, W. Wen, and Y. Zhang, A Novel Consistent-Robust SINS/GNSS/NHC Integrated Navigation Method for Autonomous Vehicles Under Intermittent GNSS Outage. *IEEE Transactions on Intelligent Vehicles*, 2024, pp. 1–17.
21. Watson, R. M. and J. N. Gross, *Robust Navigation In GNSS Degraded Environment Using Graph Optimization*, 2018.
22. Agarwal, P., G. D. Tipaldi, L. Spinello, C. Stachniss, and W. Burgard, Robust map optimization using dynamic covariance scaling. In *2013 IEEE International Conference on Robotics and Automation*, 2013, pp. 62–69.
23. Vanli, O. A. and C. N. Taylor, Robust error estimation based on factor-graph models for non-line-of-sight localization. *EURASIP JOURNAL ON ADVANCES IN SIGNAL PROCESSING*, Vol. 2022, No. 1, 2022.
24. Zhou, Y., X. Chen, and M. Ge, Robust Factor Graph Optimization Integrated Navigation Based on Improved Chi-Square Test. In *2023 International Conference on Sensing, Measurement and Data Analytics in the era of Artificial Intelligence (ICSMD)*, 2023, pp. 1–6.
25. Suenderhauf, N., M. Obst, G. Wanielik, and P. Protzel, Multipath mitigation in GNSS-based localization using robust optimization. In *2012 IEEE Intelligent Vehicles Symposium*, 2012, pp. 784–789.
26. Qin, H., X. Wang, G. Wang, M. Hu, Y. Bian, X. Qin, and R. Ding, A novel INS/USBL/DVL integrated navigation scheme against complex underwater environment. *Ocean Engineering*, Vol. 286, 2023, p. 115485.
27. Cui, X., Q. Sun, Y. Li, Z. Guo, and A. Noureldin, Vehicle Heading Enhancement Based on Adaptive Sliding Window Factor Graph Optimization for Gyroscope/Magnetometer. *IEEE Transactions on Instrumentation and Measurement*, Vol. 73, 2024, pp. 1–14.
28. Engel, J., V. Koltun, and D. Cremers, Direct Sparse Odometry. *IEEE Transactions on Pattern Analysis and Machine Intelligence*, Vol. 40, No. 3, 2018, pp. 611–625.
29. Xu, T., X. Xu, D. Xu, Z. Zou, and H. Zhao, A New Robust Filtering Method of GNSS/MINS Integrated System for Land Vehicle Navigation. *IEEE Transactions on Vehicular Technology*, Vol. 71, No. 11, 2022, pp. 11443–11453.
30. Silva, D. C., A. Frutuoso, L. F. Souza, and E. A. de Barros, Comparative Analysis of Innovation-Based Adaptive Kalman Filters Applied to AUVs Navigation. In *2022 Latin American Robotics Symposium (LARS), 2022 Brazilian Symposium on Robotics (SBR), and 2022 Workshop on Robotics in Education (WRE)*, 2022, pp. 31–36.

31. Zheng, X., Y. Dong, Y. Zhao, B. Zhang, and M. Li, TSF-GINS: Based on time-fixed sliding window with factor graph a global navigation satellite system and inertial measurement unit tightly coupled localization system. *Measurement*, Vol. 239, 2025, p. 115421.

32. Tang, H., T. Zhang, X. Niu, J. Fan, and J. Liu, Impact of the Earth Rotation Compensation on MEMS-IMU Preintegration of Factor Graph Optimization. *IEEE Sensors Journal*, Vol. 22, No. 17, 2022, pp. 17194–17204.